AD-A067 060 FOREIGN TECHNOLOGY DIV WRIGHT-PATTERSON AFB OHIO F/G 20/4
CALCULATION OF A SUPERSONIC FLOW AROUND A COOLABLE SPHERE USING--ETC(U)
JUN 78 B M PAVLOV

UNCLASSIFIED FTD-ID(RS)T-0814-78 NL

| OF |
AD
A067060

END
DATE
FILMED
6-79
DDC

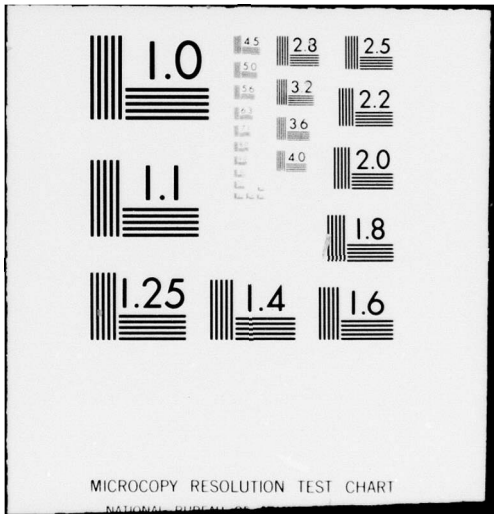
1.0
1.1
1.25
1.4
1.6
1.8
2.0
2.2
2.5
2.8
3.2
3.6
4.0
4.5
5.0
MICROCOPY RESOLUTION TEST CHART

FTD-ID(RS)T-0814-78

1

FOREIGN TECHNOLOGY DIVISION

CALCULATION OF A SUPERSONIC FLOW AROUND A COOLABLE SPHERE USING THE COMPLETE NAVIER-STOKES EQUATIONS

by

B. M. Pavloa

EDITED TRANSLATION

FTD-ID(RS)T-0814-78 2 June 1978

MICROFICHE NR: FTD-78-C-000745

CALCULATION OF A SUPERSONIC FLOW AROUND A COOLABLE SPHERE USING THE COMPLETE NAVIER-STOKES EQUATIONS

By: B. M. Pavlov

English pages: 15

Source: Vychislitel'nyye Metody i Programmirovaniye, Vol. 15, 1970, pp. 19-30

Country of origin: USSR
Translated by: Victor Mesenzeff
Requester: FTD/TQTA
Approved for public release; distribution unlimited.

PREPARED BY:

TRANSLATION DIVISION
FOREIGN TECHNOLOGY DIVISION
WP-AFB, OHIO.

U. S. BOARD ON GEOGRAPHIC NAMES TRANSLITERATION SYSTEM

Block	Italic	Transliteration	Block	Italic	Transliteration
А а	*А а*	A, a	Р р	*Р р*	R, r
Б б	*Б б*	B, b	С с	*С с*	S, s
В в	*В в*	V, v	Т т	*Т т*	T, t
Г г	*Г г*	G, g	У у	*У у*	U, u
Д д	*Д д*	D, d	Ф ф	*Ф ф*	F, f
Е е	*Е е*	Ye, ye; E, e*	Х х	*Х х*	Kh, kh
Ж ж	*Ж ж*	Zh, zh	Ц ц	*Ц ц*	Ts, ts
З з	*З з*	Z, z	Ч ч	*Ч ч*	Ch, ch
И и	*И и*	I, i	Ш ш	*Ш ш*	Sh, sh
Й й	*Й й*	Y, y	Щ щ	*Щ щ*	Shch, shch
К к	*К к*	K, k	Ъ ъ	*Ъ ъ*	"
Л л	*Л л*	L, l	Ы ы	*Ы ы*	Y, y
М м	*М м*	M, m	Ь ь	*Ь ь*	'
Н н	*Н н*	N, n	Э э	*Э э*	E, e
О о	*О о*	O, o	Ю ю	*Ю ю*	Yu, yu
П п	*П п*	P, p	Я я	*Я я*	Ya, ya

*ye initially, after vowels, and after ъ, ь; e elsewhere.
When written as ё in Russian, transliterate as yё or ё.

RUSSIAN AND ENGLISH TRIGONOMETRIC FUNCTIONS

Russian	English	Russian	English	Russian	English
sin	sin	sh	sinh	arc sh	$\sinh^{-1}$
cos	cos	ch	cosh	arc ch	$\cosh^{-1}$
tg	tan	th	tanh	arc th	$\tanh^{-1}$
ctg	cot	cth	coth	arc cth	$\coth^{-1}$
sec	sec	sch	sech	arc sch	sech^{-1}
cosec	csc	csch	csch	arc csch	csch^{-1}

Russian	English
rot	curl
lg	log

CALCULATION OF A SUPERSONIC FLOW AROUND A COOLABLE SPHERE USING THE COMPLETE NAVIER-STOKES EQUATIONS

B. M. Pavlov

This work [1] presents a statement and a numerical solution for a problem of a stationary flow around blunt solids by a supersonic flow of a low-density gas. The method is based on a finite-difference approximation of the complete nonstationary Navier-Stokes equations for a compressible gas and on finding a stationary solution as a result of the determination. Works [1]–[3] present the initial calculation results and examine certain methodological problems which characterize the numerical algorithm. Work [4] contains the calculation results for a flow past a heat-insulated sphere. This work discusses a pattern of flow around a coolable sphere under the conditions of small Reynolds numbers.

Designations: r, θ - spherical polar system of coordinates (Fig. 1); r_w - sphere radius; W - flow velocity vector; u, v - its components with respect to r and θ; ρ, h, T, p - density, enthalphy, temperature, and pressure; λ, μ - coefficients of heat conductivity and shear viscocity; γ - ratio of specific heats; q - heat flow to the wall; τ - friction tension; F - force of resistance; C_D - coefficient of total resistance; C_f - friction coefficient; l - mean free path of molecules; Re, M_∞, Kn, Pr - numbers of Reynolds, Mach, Knudsen, and Prandl; d, I - thickness and intensity of a shock wave; p_0 - stagnation pressure behind a normal shock;

r_* - sonic line; subscripts: ∞ - in an incident flow, w - on the sphere surface, s - behind a normal inviscid shock, 0 - flow stagnated adiabatically and isentropically, ПС - in a boundary layer, СМ - in a free-molecular flow; superscripts: 0 - in the leading critical point, * - along the boundary ray θ^*.

1. An examination is made of a viscous gas flow, which is uniform and supersonic at infinity, around a sphere. The problem concerning the calculation of the flow field is solved under the following assumptions: 1) the gas flowing past the sphere is thermically and calorically ideal, 2) the coefficients λ and μ are power functions of enthalpy $(\sim h^\omega, 0{,}5 \leqslant \omega \leqslant 1)$, 3) the flow has a laminar nature at small Reynolds numbers, and 4) under these conditions of flow the Navier-Stokes equations for the compressible gas are valid in the entire area outside the sphere.

Conditions 1) and 2) lead to constant values of the numbers γ and Pr. Dimensionless variables are used: linear dimensions pertain to r_w, velocities - to W_∞, density - to ρ_∞, enthalpy - to W_∞^2, pressure and tension of friction - to $\rho_\infty W_\infty^2$, heat flow - to $\rho_\infty W_\infty^3$, and force of resistance - to $1/2\pi r_w^2 \rho_\infty W_\infty^2$.

Work [1] shows the initial system of equations in a dimensionless form relative to the unknowns ρ, u, v, h, p, and μ in the system of coordinates r, θ. Since with a laminar nature the flow has a symmetry relative to the $\theta=0$ axis, it is sufficient to seek a solution for the problem in the region $r \geqslant 1$, $0 \leqslant \theta \leqslant \pi$. According to the systematic investigations, which are described briefly in [1] and [3], numerical integration can be accomplished in the end region (Fig. 1) $1 \leqslant r \leqslant R_2$, $0 \leqslant \theta \leqslant \theta^*$, where $R_2 = R_2(\theta)$ - given equation for the surface of rotation (in this case, of an ellipsoid whose left focal point is congruent with the center of the sphere), θ^* - position of the boundary ray $(0 < \theta^* \leqslant \pi)$.

Let us formulate the boundary conditions of the problem. The conditions of the uniformity of the flow at an infinite distance from the sphere are removed to the surface $R_2(\theta)$, $0 \leqslant \theta \leqslant \theta^*$. On the sphere the enthalpy (temperature) of the surface coincides with the enthalpy of gas and is equal to the value h_w (there is no jump in temperature) and both velocity components are equal to zero

(there is no slip). On the axis $\theta=0$, $\theta=\pi$ we use the conditions of symmetry of the flow. If $\theta^*<\pi$, it is necessary to assign conditions for the functions u, v, h along the ray $\theta=\theta^*$. By means of series of calculations with a varied position of the angle $\theta^*, 0<\theta^*<\pi$ it was established that, when assigning the approximate conditions for these functions in the form of $\partial^2 f/\partial\theta^2=0$ (i. e., a linear change in f in the vicinity of the ray θ^*) there is an insignificant reverse effect of the flow. In this case the density $\rho(r, \theta^*)$ can be found from an analogous condition or from a continuity equation.

The finite-difference approximation of the initial equations and boundary conditions, and also the peculiarities of the numerical algorithm, are described in [1]–[3].

2. The study of the super- and hypersonic flow around blunt solids with the cooling of their surface ($h_w<h_o$) is of practical interest in connection with the problem of heat protection for a flying vehicle. Below we'll discuss the characteristic peculiarities of the viscous gas flow near the sphere placed in a supersonic flow of a diatomic ideal gas ($\gamma=1$, 4 Pr=0.72, $\omega=3/4$, $h_w=0.3$). The effect of the M_∞ and Re_∞ numbers has been studied on the flow pattern under the conditions of flow and heat exchange, which are indicated in the table. The same table shows the Knudsen Kn and Reynolds Re_s (calculated using the parameters behind the normal shock) numbers which characterize the degree of rarefcation of the incident flow:

$$Re_s = \frac{\rho_s u_s r_w}{\mu_s} = \frac{Re_\infty}{\bar{\mu}_s} = \frac{Re_\infty}{M_\infty^{2\omega}} \left[\frac{\bar{\rho}_s(\gamma+1)}{2\gamma-(\gamma-1)/M_\infty^2}\right]^\omega,$$

$$\bar{\rho}_s = \frac{\rho_s}{\rho_\infty}, \quad \bar{\mu}_s = \frac{\mu_s}{\mu_\infty}, \quad Kn = \frac{l_\infty}{r_w} = \frac{16}{5}\sqrt{\frac{\gamma}{2\pi}} \cdot \frac{M_\infty}{Re_\infty}.$$

With an increase in rarefaction there is an increase in the Kn number and a decrease in Re_s. In most calculations $\theta^*=99^\circ$.

Let's briefly describe the behavior of the gas-dynamic parameters at the leading critical point in the area where the shock wave is thickened and in a compressed layer behind it, and also along the surface of the sphere. Since the calculations were accomplished for the flow conditions which occupy the intermediate position

between the flows of the solid and free-molecular media, it is of interest to compare the results of the calculation with the corresponding theoretical results and experiments in rarefied gases.

1. Leading critical point. The solid line in Fig. 2, a represents the behavior of the ratio p_w°/p_o', which characterizes the deviation of the calculated pressure from the pressure in an inviscid flow, as a function of $Re_s\sqrt{\bar{\rho}_s}$. With a decrease in the parameter $\eta = Re_s\sqrt{\bar{\rho}_s}$ (introduced for a convenience of the comparison with the experimental data [5], shaded area in this figure) the values of p_w°/p_o' begin to increase approximately from $\eta=100$, which is in good agreement with the experiments and the theory of free-molecular flows [6] (with $Re_s=0$, $\gamma=1.4$ and totally diffused deflection of the molecules from a hard, very cold wall the ratio p_{CM}/p_o' attains a value equalling to 1.087). An increase in pressure is the result of merging of the thickened boundary layer and shock wave.

The solid line in Fig. 2, b shows the behavior of the ratio q_w°/q_{nc}° as a function of the Re_s number. This ratio characterizes the difference in heat transfer in a flow of rarefied gas and in flows with large Reynolds numbers. The value q_{nc}° was calculated by the Fay and Riddell formula [7], and

$$q_w(\theta) = \frac{1}{Pr\,Re_\infty}\left(\mu\frac{\partial h}{\partial r}\right)_w,\quad 0<\theta<\theta^*.$$

According to the theory of free-molecular flow $q_{CM}^\circ=1/2$ and the ratio $q_{CM}^\circ/q_{nc}^\circ$, which is proportional to $\sqrt{Re_\infty}$, approaches zero with an increase in rarefaction. The same figure shows the following: the shaded area - data of a series of experiments (borrowed from [5], the dot-dash line - $q_{CM}^\circ/q_{nc}^\circ$, the dashed line - the curve $q_w^\circ/q_{nc}^\circ = 1+0.52/\sqrt{Re_\infty}$ obtained in [8] by processing the measurements (the conditions of this experiment are close to the conditions of these calculations: $M_\infty=2$, 4, 6; $20\lesssim Re_s\lesssim 800$, $T_w/T_o\approx 0.33$). In most of the experiments carried out to determine heat transfer the value q_w°/q_{nc}° has the following nature of change: with a decrease in Re_s $(0\leqslant Re_s\leqslant 10^3)$ this value increases, here $q_w^\circ > q_{nc}^\circ$, attains

a maximum at certain $\bar{Re}_s$ $(10 \leqslant \bar{Re}_s \leqslant 10^2)$, and then decreases $(q^0_\infty < q^0_{пс}$ when $Re_s \leqslant 10)$. The calculated values of $q^0_\infty / q^0_{пс}$ detect a similar behavior; although they begin to decrease when $Re_s \leqslant 10$, they still remain higher than those determined in the experiments (with the same Re_s number). Apparently, at low Reynolds numbers, $Re_s < 10^2$, one should take into account in the calculation the conditions of slip and temperature jump on the wall, which, in particular, lead to a decrease in the values of the heat flow [9].

With a decrease in the Re_s number the density ρ^0_w increases in proportion to p^0_w since the h_w is constant (with thermal insulation a drop was observed in the density at the leading critical point [4] and [10]).

2. Shock wave structure. The thickness of a shock wave in a viscous gas is usually determined by the formula proposed by Prandl:

$$d = \frac{f_s - f_\infty}{(\partial f/\partial r)_{max}},$$

where f - any of the gas-dynamic functions, $\partial f/\partial r$ - maximum slope of the profile f to the axis $\theta=0$. In most of the experiments carried out to study the shock-wave structure (for example, [11] and [12]) the density field was measured and, therefore, thickness d was calculated using the profile ρ in the area of the shock wave. However, under the cooling conditions of the surface the calculated density profiles $\rho(r, 0)$ in the shock wave have a complex behavior (see Figs. 4 and 5) and it is difficult to use them for the calculation of d. For this it is more convenient to use the profiles $u(r, 0)$ and $p(r, 0)$, which have approximately the same nature as with thermal insulation. The calculation of the thickness of the shock wave using the profiles $u(r, 0)$, when $M_\infty=6$ and $Re_\infty=300$, 200, 90, 45, and 20, yield the following values: d=0.055; 0.084; 0.169; 0.286; and 0.474. Thus, with an increase in rarefaction the shock wave thickens quickly. The comparison of the thickness d in cases of thermal insulation and cooling (with all other conditions being equal) indicates a somewhat lesser thickness in the case of cooling. The thickness of the transition zone in the shock wave, when there is a change in the angle θ, can be determined conditionally by the

value $D(\theta)=r_1(\theta)-r_2(\theta)$, where r_1 and r_2 are points at the fixed ray θ: in r_1 the value $p-p_\infty \approx 0.01\, p_\infty$, in r_2 the $\partial p/\partial r$ attains a maximum value in the shock wave. The position of the washed out shock wave relative to the sphere can then be determined by the middle line r_D of the indicated zone. The dot-dash curve on Fig. 6 shows the position of the line r_D when $Re_\infty=45$ and $M_\infty=6$. This line travels in approximately the same way as a shock wave during an inviscid flow but it is located further from the sphere. A similar behavior of the shock wave zone was observed in an experiment (see [5]). With a change in the numbers M_∞ and Re_∞ the behavior of the value $\Delta=r_D-1$, which can be roughly considered as the "departure" of the shock wave, has the following feature: a) with a decrease in the number Re_∞ (M_∞, θ are constant) Δ increases; b) with an increase in θ (Re_∞, M_∞ are constant) Δ increases; c) with a change in the number M_∞ (θ, R_∞ are constant) this function is not monotonic (see Fig. 4): for $2 \leqslant M_\infty \leqslant 4$ the Δ diminishes, for $M_\infty>4$ it increases (the same behavior was observed in the calculations of a thermoinsulated sphere [4]). The shock wave intensity was determined by the value of the ratio $I(\theta)=(p_{max}-p_\infty)/(p_0'-p_\infty)$, where p_{max} is the value of maximum pressure in the area of the shock wave at the fixed ray θ. It was found that with an increase in θ the function $I(\theta)$, for all the flow conditions examined, decreases (for example, when $M_\infty=6$; $I(0)=0{,}917;\ I\left(\frac{\pi}{2}\right)=0{,}238$ for $Re_\infty=200$ and $I(0)=0{,}882,\ I\left(\frac{\pi}{2}\right)=0{,}193$ for $Re_\infty=45$).

Thus, with an increase in the angle θ and a decrease in the Re_∞ number, there is a continuous (according to r) washing out and weakening of the shock wave (just as in the case of thermal insulation [1]-[3]).

3. Structure of a compressed layer. Figure 3 (a, b, c) shows a typical behavior of the flow parameters in a compressed layer ($M_\infty=8$, $Re_\infty=90$), where, for comparison, the dashed lines show the solution when $\theta=0$ in the case of thermal insulation of the sphere. From an analysis of the calculated data we draw the following conclusions. The enthalpy $h(r, \theta)$ has a maximum on each ray θ due to

the cooling of the sphere's surface. The density $\rho(r, \theta)$ has a local maximum immediately behind the shock wave as it moves away from the region of the leading critical point, and maximum pressure $p(r, \theta)$ is attained between the shock wave and wall; with the low values of θ the maximum pressure $p(r, \theta)$ is on the wall. With a relatively large Re_s numbers (for example, when $M_\infty=2$ and $Re_\infty=500$) there is an area close to the sphere's surface in which the pressure along the normal to the wall changes insignificantly, which indicated the existance of a region of the type of a boundary layer.

The position of the sonic line $r_*(\theta)$ is depicted in Fig. 6 for the various Re_∞ ($M_\infty=6$, solid lines) numbers and in Fig. 8 for the various M_∞ ($Re_\infty=90$, solid lines) numbers. It is evident that with a change in θ and M_∞ (Re_∞ is constant) the behavior of these lines is nonmonotonic. For a constant M_∞ number sonic lines move further away from the sphere's surface with a decrease in the Re_∞ number.

Let us examine in more detail the behavior of the solution along the stagnation line $\theta=0$. Figure 4 characterizes the behavior of u and ρ with a change in the M_∞ ($Re_\infty=90$) number. Using profiles $u(r, 0)$ we can clearly see the nonmonotonic nature of "departure" of the shock wave noted above. The density increases along the $\theta=0$ axis when $r \to 1$; here there are regions of sharp increase of ρ in the shock wave and close to the body (the latter is the result of cooling of the surface). Both these regions have a tendency to merge with an increase in the M_∞ number and the fixed Re_∞ number (i. e., with a decrease in the Re_s number) (Figs. 4 and 5).

Figure 5 shows the distribution of the density $\rho(r, 0)$ and enthalpy $h(r, 0)$ when $M_\infty=6$ and a change in the Re_∞ number. It is evident that with a decrease of the Re_∞ number (and, consequently, Re_s number) the maximum value of $h(r, 0)$, which is achieved behind the shock wave, also decreases and $h_{max}<h_s$. If we take the point r, where the maximum $h(r, 0)$ is achieved, to be the trailing front of the washed-out shock wave, it turns out that, at this point, the density $\rho(r, 0)<\rho_s$ and $p(r, 0)<p_s$, i. e., an incomplete compression in the shock wave, leads to disruption of the Renkin-Hugoniot conditions and to its gradual disintegration with an increase in rarefaction. With an increase in rarefaction its gradual thicken-

ing is evident in the area of the shock wave according to the profiles of h(r, 0). Approximately the same behavior of the density and temperature was observed along the line of stagnation in the experiment of work [13], in which nitrogen flowed past a cylinder with a spherical blunt end (M_∞=9, Kn=0.045, T_0=298°K, and $T_w/T_0 \approx 0.3$). The field temperatures determined in [3] attest to the presence of a noticeable temperature jump on the model surface (T_w^0/T_0=0.78 when $T_w/T_0 \approx 0.3$ at the leading critical point).

4. Distributions along the surface of the sphere. Figure 7 shows the graphs of the deduced pressure $\bar{p}_w = p_w(\theta)/p_w(0)$ and heat flow $q_w(\theta)$ when M_∞=6 and with different values of the Re_∞. In the same figure the dot-dash line depicts the function $q_{CM}=\cos\theta/2$, the dotted line - $q_{пс}(\theta)$, obtained from the calculation of the boundary layer on the sphere [14] ($M_\infty=10$, $Re\sim10^6$, $\gamma=1{,}4$, $T_w/T_0=0{,}6$), the dashed line - $\bar{p}_w(\theta)$ when $M_\infty=6$, $Re_\infty=\infty$ ([7], chapter 8). With a decrease in the Re_∞ number the values of $\bar{p}_w$ gradually increase on the front section of the sphere and they are higher than the corresponding values in an inviscid flow. With an increase in the angle θ the function $q_w(\theta)$ decreases gradually and with a decrease in the Re_∞ the values of $q_w(\theta)$ increase; in this case, $q_{пс} < q_w < q_{см}$. The nature of change in the calculated heat flow is in agreement with the experiments [8] and [15].

Figure 8 shows the friction coefficient graphs $C_f = \tau_w/\rho_\infty W_\infty^2 = Re_\infty^{-1}(\mu\,\partial v/\partial r)_w$ for Re_∞=90 and the various M_∞ numbers (solid lines). In the same figure the dot-dash line depicts the function $[C_f(\theta)]_{см} = (\sin 2\theta)/2$, the dashed line - $[C_f(\theta)]_{пс}$ taken from work [14]. All calculation curves of $C_f(\theta)$ are located between the curves for the free-molecular and boundary-layer conditions of flow. The values of C_f increase with a decrease in the Re_∞ number. With a change in the angle θ the function $C_f(\theta)$ has a maximum for the various Re_∞ numbers when $\theta \sim 40$–60 degrees, i. e., about in the middle of the area of a sharp approch of the sonic line to the sphere. In the calculations of the boundary layer on blunted solids [16] it was found that the maximum values of the function $C_f(\theta)$ were obtained in the vicinity of the sonic point on the surface

of the streamlined body. The behavior of the functions $\bar{p}_w$ and C_f is analogous to the case of thermal insulation when there is a decrease in the Re_∞ number [4].

Figure 9 shows the construction of the ratio $C_D/(C_D)_{CM}$ as a function of the number $2Re_s$, the shaded areas indicate the data of the experiments carried out to determine the resistance of spheres [5]. The quantity C_D was calculated by the formula $C_D = 4\int_0^{\theta^*} (p_w \cos\theta + C_f \sin\theta) \sin\theta \, d\theta$, and $(C_D)_{CM}$ by the formula used to calculate the diffused deflection with the accommodation coefficient equalling unity [6]. It is obvious that in the examined conditions of flow $C_D < (C_D)_{CM}$, while the ratio being examined increases with a decrease in the Re_s number.

3. The numerical results indicate that when $Re_s \lesssim 10^2$ the shock wave and the boundary layer join in the area of the leading critical point of the sphere, which leads to a series of new phenomena which do not take place in flows with large Reynolds numbers. With reduced rarefaction the calculated aerodynamic characteristics have a tendency to approach the corresponding values in a free-molecular flow and, in the range $10 \lesssim Re_s \lesssim 10^2$, there is a satisfactory agreement between them and the measurements derived from the experiments. When $Re_s \lesssim 10$ there is a certain anomaly in the behavior of some characteristics of the flow, which can be explained by the fact that the effects of slip and temperature jump were disregarded in these calculations. Apparently, when taking these effects into consideration within the framework of the Navier-Stokes model, there should be a better agreement with the experiments also at lower Reynolds numbers ($Re_s < 10$). The same conclusions are drawn from the analysis of flows with thermal insulation of the sphere's surface [4]. Thus, one can assert that the numerical solutions of the problem of flow in this setting afford the description of the phenomena in a compressed layer, which are close to those observed in experiments.

The author expresses his appreciation to Z. M. Yemel'yanov and L. V. Kuznetsov who took part in calculations and processing of the

results.

BIBLIOGRAPHY

1. Павлов Б. М. Численное решение задачи о сверхзвуковом обтекании ограниченных затупленных тел с помощью полных уравнений Навье — Стокса. Научный отчет № 93—3а (350). ВЦ МГУ, 1967.
2. Павлов Б. М. Численное решение задачи о сверхзвуковом вязком течении газа около затупленных тел. В сб.: «Вычислительные методы и программирование», вып. XI. Изд-во МГУ, 1968.
3. Павлов Б. М. О расчете сверхзвукового обтекания затупленных тел с использованием полных уравнений Навье — Стокса. «Изв. АН СССР», сер. механ. жидк. и газа, 1968, № 3.
4. Павлов Б. М. Применение полных уравнений Навье — Стокса к расчету сверхзвукового обтекания теплоизолированной сферы. Тр. II Всесоюзн. семинара «Вычислительные методы механики вязкой жидкости». Новосибирск, Изд-во СО АН СССР, 1969.
5. Potter J. L. The transitional rarefied flow regime. Rarefied das dynamics (ed. by C. L. Brundin), v. 2, Acad. Press, N. Y.— London, 1967.
6. Хейз У. Д., Пробстин Р. Ф. Теория гиперзвуковых течений. М., ИЛ, 1962, гл. X.
7. Фей Д., Ридделл Ф. *Теоретический анализ теплообмена в передней критической точке, омываемой диссоциированным воздухом.* В сб.: «Газодинамика и теплообмен при наличии химических реакций». М., ИЛ, 1962.
8. Хикман Р., Гайдт У. Теплоотдача к цилиндрам со сферическим носком при низких значениях чисел Рейнольдса. «Ракетн. техн. и косм.», 1963, т. 1, № 3.
9. *Основы газовой динамики (под ред. Г. Эммонса).* М., ИЛ, 1963, *гл.* VIII.
10. Иванов А. В. Экспериментальное исследование влияния чисел Маха и Рейнольдса на структуру сверхзвукового потока разреженного газа в окрестности передней критической точки затупленного тела. «Изв. АН СССР», сер. механ. жидк. и газа, 1967, № 3.
11. Иванов А. В. Структура ударной волны в воздухе при числах Маха от 2,6 до 6. «Изв. АН СССР», сер. механ. жидк. и газа, 1967, № 2.
12. Robben F., Talbot L. Measurements of shock wave thickness by the electron beam fluorescence method — Phys. Fluids, 1966, v. 9, No. 4.
13. Тирумалеса Д. Экспериментальное исследование гиперзвукового обтекания затупленного тела разреженным газом. «Ракетн. техн. и косм.», 1968, т. 6, № 2.
14. Davis R., Flugge-Lotz J. Second order boundary layer effects in hypersonic flow past axisymmetric blunt bodies. J. Fluid Mech., 1964, v. 20, No. 4.
15. Ferri A., Zakkay V., Ting L. Blunt-body heat transfer at hypersonic speed and low Reynolds numbers. JAS, 1961, v. 28, No. 12.
16. Башкин В. А., Колина Н. П. Ламинарный пограничный слой на эллипсоидах вращения. «Изв. АН СССР», сер. механ. жидк. и газа, 1966, № 6.
17. Белоцерковский О. М. и др. Обтекание затупленных тел сверхзвуковым потоком газа. «Тр. ВЦ АН СССР». М., 1966.

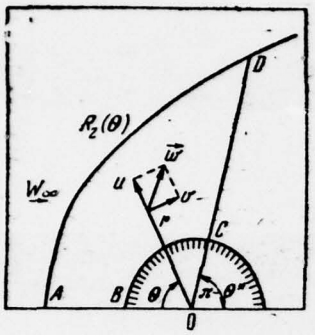

Fig. 1.

Table

M_∞	Re_∞	h_w/h_0	Re_s	Kn
2	500	0,267	338	0,006
2	90	0,267	61	0,033
4	300	0,457	105	0,020
4	90	0,457	32	0,067
6	300	0,527	63	0,030
6	200	0,527	42	0,045
6	90	0,527	19	0,100
6	45	0,527	9,5	0,200
6	20	0,527	4,2	0,450
8	90	0,557	13	0,133

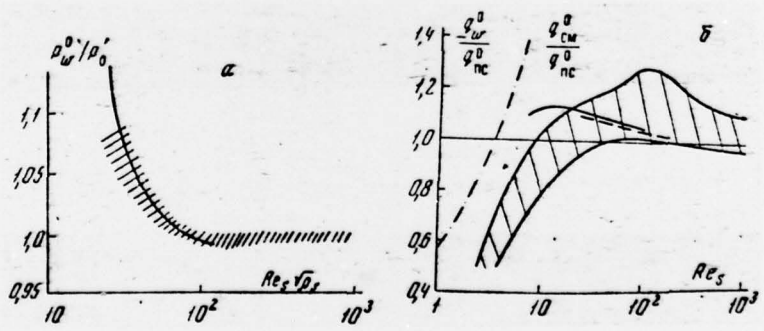

Fig. 2. Behavior of p^0_w/p'_0 (a) and $q^0_w/q^0_{пс}$ (b) at the leading critical point.

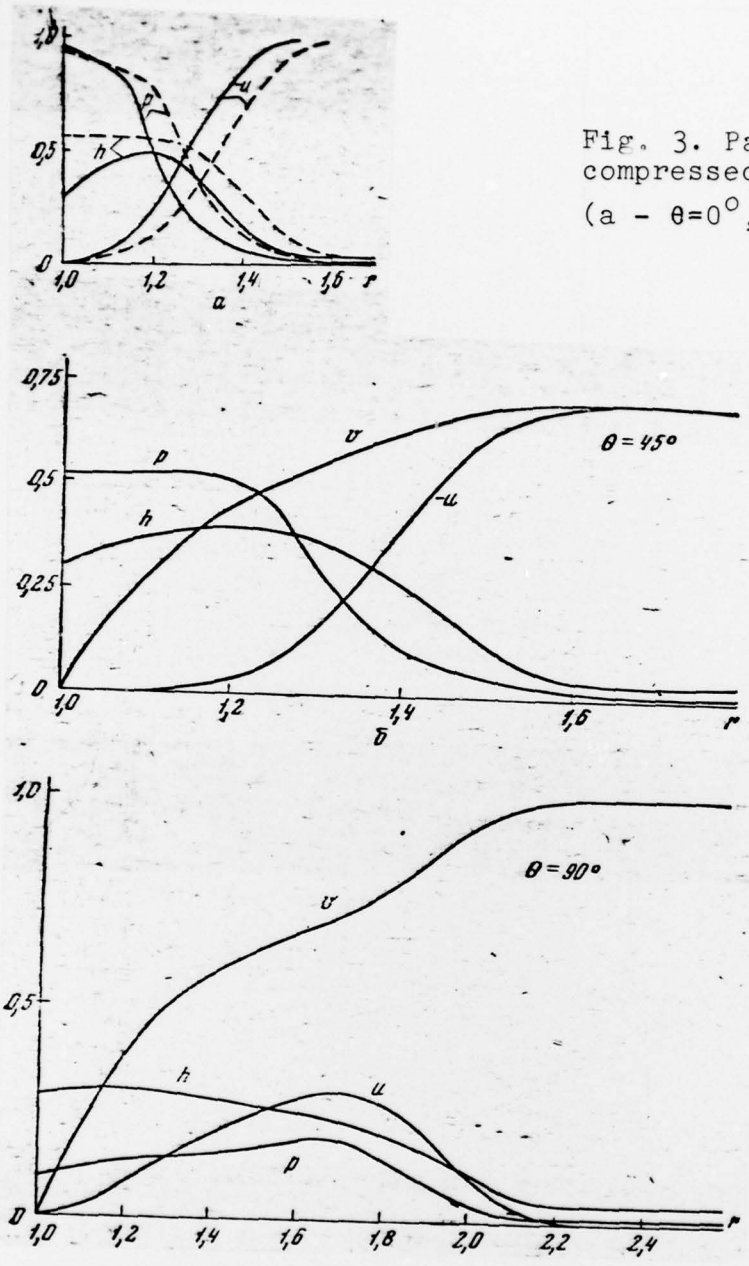

Fig. 3. Parameters of flow in a compressed layer. $M_\infty=8$, $Re_\infty=90$ (a - $\theta=0^\circ$, b - $\theta=45^\circ$, c - $\theta=90^\circ$)

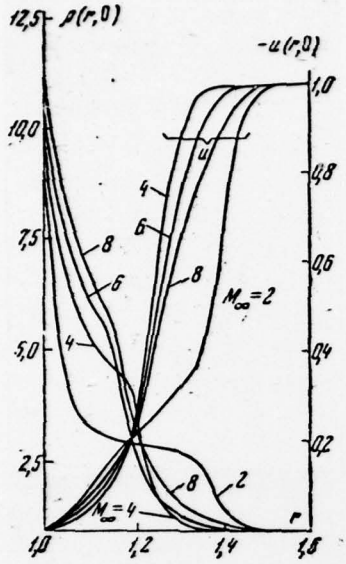

Fig. 4. Profiles of functions ρ and u on the stagnation line θ=0 (Re_∞=90)

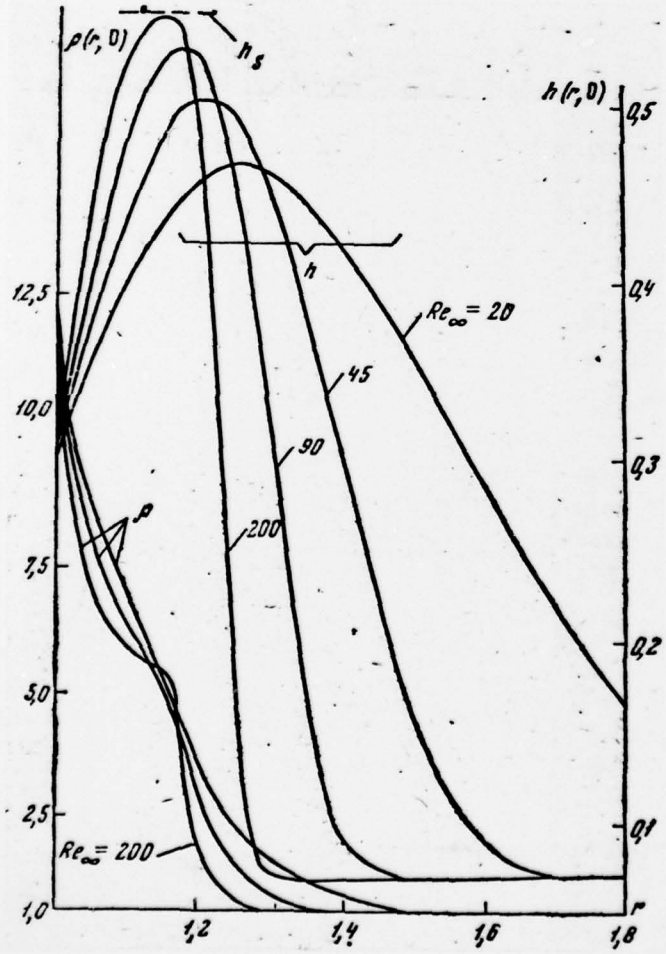

Fig. 5. Profiles of functions ρ and h on the stagnation line θ=0 (M_∞=6)

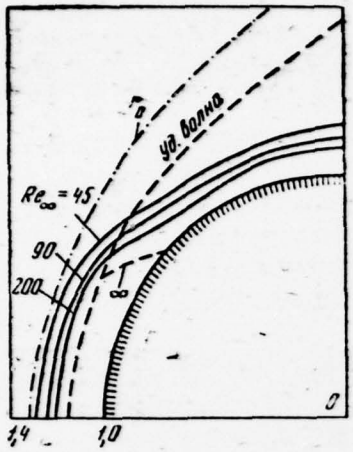

Fig. 6. Sonic lines, $M_\infty=6$

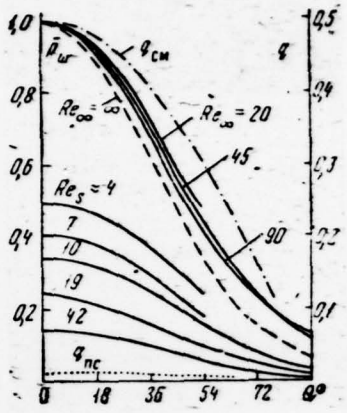

Fig. 7. Distribution of pressure $\bar{p}_w$ and heat flow q_w on the sphere

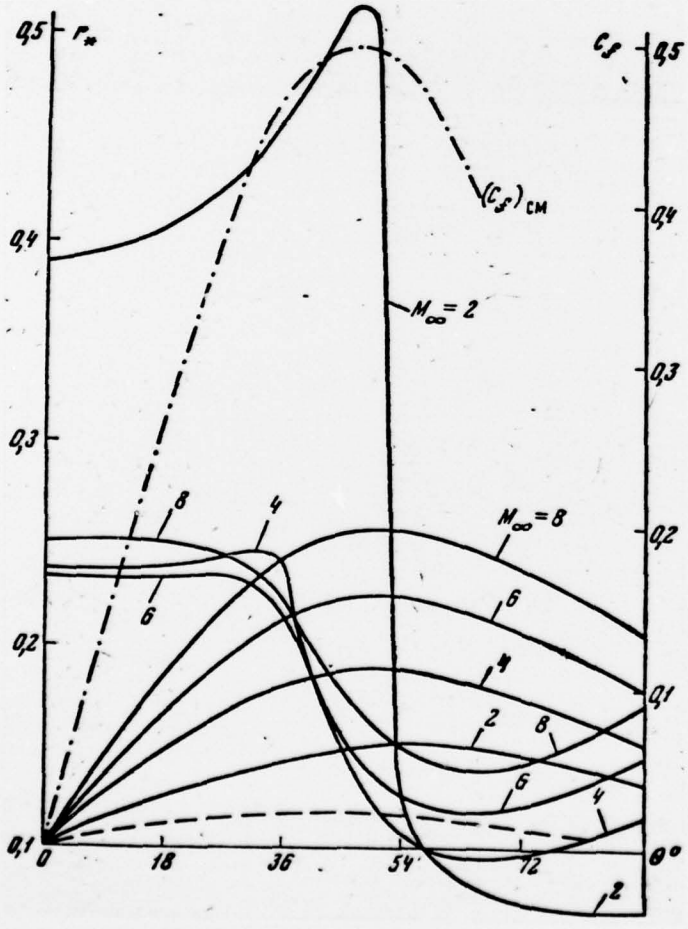

Fig. 8. Sonic lines r_* and friction coefficient $C_f(Re_\infty=90)$

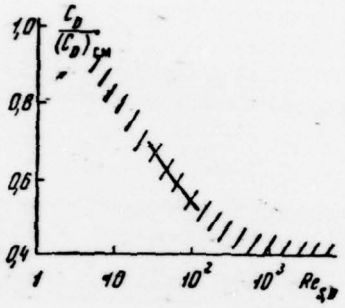

Fig. 9. Sphere resistance coefficient

DISTRIBUTION LIST

DISTRIBUTION DIRECT TO RECIPIENT

ORGANIZATION		MICROFICHE
A205	DMATC	1
A210	DMAAC	2
B344	DIA/RDS-3C	8
C043	USAMIIA	1
C509	BALLISTIC RES LABS	1
C510	AIR MOBILITY R&D LAB/FIO	1
C513	PICATINNY ARSENAL	1
C535	AVIATION SYS COMD	1
C591	FSTC	5
C619	MIA REDSTONE	1
D008	NISC	1
H300	USAICE (USAREUR)	1
P005	ERDA	1
P055	CIA/CRS/ADD/SD	1
NAVORDSTA (50L)		1
NASA/KSI		1
AFIT/LD		1

ORGANIZATION		MICROFICHE
E053	AF/INAKA	1
E017	AF/ RDXTR-W	1
E404	AEDC	1
E408	AFWL	1
E410	ADTC	1
E413	ESD	2
	FTD	
	CCN	1
	ASD/FTD/NICD	3
	NIA/PHS	1
	NICD	2